Synthesis and characterization of $Dy_3Fe_5O_{12}$ nanoparticles fabricated with the anion resin exchange precipitation method

R. Ivantsov[a*], N. Evsevskaya [b], S. Saikova [c], E. Linok [b], G. Yurkin [a,c], I. Edelman[a]

[a]*Kirensky Institute of Physics, FRC KSC RAS, Krasnoyarsk, 660036, Russia*
[b]*Institute of Chemistry and Chemical Technology FRC KSC SB RAS*
Krasnoyarsk, 660036, Russia
[c]*Siberian Federal University, Krasnoyarsk, 660041, Russia*

ABSTRACT
Dysprosium-iron garnet (DyIG) nanoparticles were synthesized with the new modification of the anion resin exchange precipitation method. Nanoparticles structure and morphology were characterized by the Fourier transform infrared spectroscopy (FT-IR), X-ray diffraction (XRD), and transmission electron microscopy (TEM). The magnetic properties were studied by using a QUANTUM Design MPMS-XL system and the visible magnetic circular dichroism (MCD). The nanoparticles synthesized were of the garnet structure with an excellent crystallinity. Nanoparticles magnetic properties were close to that of the bulk DyIG crystals. Nanoparticles magnetization dependence on an external magnetic field demonstrates narrow hysteresis loop and the strong magnetization increase in high fields. Visible MCD of DyIG was studded here for the first time. The MCD spectral and temperature dependences allowed to separate contributions of the Fe and Dy sub-lattices to this effect and to analyze each sub-lattice temperature behavior.

1. Introduction

Yttrium and rare earth iron garnets ($Y_3Fe_5O_{12}$, $R_3Fe_5O_{12}$, YIG and RIG) attract inexhaustible interest since early 1950's, when Yoder and Keith obtained YIG crystal for the first time [1], and Bertaut and Forret [2], and Geller and Gilleo [3] reported magnetic properties of YIG and GdIG, correspondingly, and still. The fundamental interest is due to a great variety of the garnet physical properties, in particular, to a phenomenon of the sub-lattices magnetic moments compensation observed in most of the rare earth iron garnets [4]. On the other hand, ferrimagnetic garnets are widely applied for tunable microwave devices, circulators, isolators, phase shifters, magneto-photonic devices, etc. (for example, [5,6,7,8]). Last decades the YIG and RIG nanocrystals [9,10,11,12 ,13,14,15] have gained one of the central positions in the physics and technology of magnetism since the nano-metric state gives additional possibilities of the garnet applications. At that, the question arises on compliance of the nanoparticle properties to the

properties of bulk counterparts. From this view point, it would be interesting to study separately the temperature behavior of iron and rare earth sub-lattices. However, this question was not touched upon in papers on RIG nanoparticles available in the current literature. Visible magnetic circular dichroism (MCD) is one of the particularly informative magneto-optical effects [16], since it is observed in the relatively narrow bands at photon energies corresponding to transitions between ground and excited states of an ion in insulators or between bands in metals and semiconductors. The MCD spectral and temperature dependences are helpful for the in-depth understanding of the nanoparticles electronic structure and electronic excitations under an action of an electromagnetic irradiation. MCD is the differential absorption of electromagnetic waves polarized over the left and right circle relative to the magnetic field vector (or magnetization of a substance), oriented parallel to the direction of the wave propagation. This effect is widely used in the chemistry of both organic and complex inorganic compounds and in biological studies (for example, [17]). As a rule, MCD spectra are characterized by narrow lines, which make it possible to obtain reliable information on optical resonances, in particular, associated with electron transitions in different sub-lattices in the case of ferrimagnetic substance. However, until now, MCD has been rather rarely used to study ferro- and ferrimagnets. The series of works of G.A. Gehring with co-authors are known devoted to the MCD study of the manganite, magnetite, ZnO, and doped ZnO thin films (e.g.,[18, 19]). As concerns rare earth iron-garnet ferrites, number of authors investigated the Faraday rotation (FR) in a variety of magnetically ordered bulk garnet crystals and films (for instance, [20, 21,22]). However, the structure of the FR spectra of YIG and RIG are, as a rule, not clearly for interpretation because their origination from the overlapping contributions of the many transitions and of the dispersive nature of FR. The MCD study was carried out only for $Y_3Fe_5O_{12}$ thin films [23, 24] and slices cut from bulk crystals [25], and for $Er_3Fe_5O_{12}$ thin crystal plates [26]. $Dy_3Fe_5O_{12}$ (DyIG) is exceptionally suitable for the MCD investigation. Several narrow f-f bands in Dy^{3+} ions: $^6H_{15/2} \rightarrow {}^6F_{3/2}, \rightarrow {}^6F_{5/2}, \rightarrow {}^6(F_{7/2}$

+ $H_{5/2}$) occur in the energy region 11000-14000 cm^{-1}, where electron transitions in Fe^{3+} ions have extremely low intensities. The same area of energy represents applied interest in connection with using new laser sources of radiation for this range. On the other hand, the Dy^{3+} f-f bands are completely absent in the higher energy region where main the Fe d-d and charge transfer transitions take place. These circumstances open the possibility to study separately the temperature and field dependences of MCD of the rare-earth and iron sub-lattices.

The nanoparticle properties depend strongly, sometime critically, on the preparation conditions. A fairly complete overview of ferrite nanoparticles fabrication techniques is presented in Ref. [27]. Despite the variety of described techniques any of them is not universal; therefore, the creation of a novel or new modifications of the known techniques for obtaining Dy$_3$Fe$_5$O$_{12}$ garnet is an actual problem. Some of co-authors of the present paper reported earlier a new way to synthesize various compound nanoparticles such as α-Co(OH)$_2$, α-Ni(OH)$_2$, CoAl$_2$O$_4$, NiAl$_2$O$_4$, Y$_3$Fe$_5$O12, Y$_3$Al$_5$O$_{12}$, Dy$_2$O$_3$, using precipitation method in the presence of the strong base anion exchange resins in OH-form [28,29,30,31,32,33,34]. This technique involves anion exchange between the resin and the solution and precipitation of an insoluble compound of metal from the solution. Besides the resin sorbs impurity anions from the reaction solution, while in the case of ordinary reagent method these impurities and also ions which are derived from precipitation reagent, for example, sodium hydroxide or ammonia, remain in the product and complicate the formation of uniform particles. Also the process of anion resin exchange precipitation is carried out under controlled conditions at constant pH value. More details on the advantages of anion resin exchange precipitation are reported in [35].

To our knowledge, the anion resin exchange precipitation method was not applied earlier to prepare DyIG nanoparticles. It is worth nothing that in this study we use the anion exchange resin in CO$_3$-form, we suppose in this case the particles of smaller size and better crystallinity can be produced as compared to using the exchange resin in OH-form. The structure, morphology, magnetic and magneto-

optic properties of the synthesized nanoparticles are investigated. The study of the MCD spectral and temperature dependences allowed to separate contributions of iron and rare earth sub-lattices and analyze their behavior in the region of the magnetic compensation temperature.

2. Experimental

2.1. Synthesis of DyIG nanoparticles

Commercially available the strong base gel anion resin AV-17-8 in the chloride form with grain size 0.25 – 0.5 mm (Russian GOST 20301–74) was transformed into the CO_3^- form using its three times treatment with 1M Na_2CO_3 solution during 1 h, and extensive washing with water to neutral reaction. The total exchange capacity of the anion resin was determined using 0.1M HCl.

In a typical procedure, mixture of 9,4 ml 0.25 M $Dy(NO_3)_3$ and 15,6 ml 0.25 M $Fe_2(SO_4)_3$ was added drop wise to the 40 ml of anion resin AV-17-8 in CO_3-form under vigorous stirring for 1 h. Molar ratio Dy/Fe was 3:5. After the reaction, the anion resin beads were removed using a sieve, the precipitate was centrifuged, washed with distilled water several times and finally dried in air at 100 °C to form a precursor. Subsequently, precursor was calcined at 850 °C for 2-5 h in order to produce $Dy_3Fe_5O_{12}$.

2.2. Nanoparticles characterization

Powder X-ray diffraction was carried out using PANalytical X'pert Pro diffractometer equipped with a Cu Kα anode. Fourier transformed infrared spectra (FT-IR) were recorded on a Bruker Vector 22 spectrometer. Transmission electron microscope (TEM), Hitachi H-800, was used to characterize the morphology and microstructure of the samples.

Magnetization hysteresis loops were recorded with a QUANTUM Design MPMS-XL system at temperature 298 K with magnetic field value up to 50 kOe.

To carry out MCD measurements, transparent composite plates containing the nanoparticles were prepared: the nanoparticles powder was mixed with dielectric transparent silicon-based glue ("Rayher" art. nr. 3338100 80 ml) in the weight proportion 0.5/100 and measures were undertaken to obtain the homogeneous particles distribution in a matrix such as ultrasonic bath. The low magnetic powder concentration allowed us to exclude the interaction between nanoparticles. The mixture was placed between two thin glass plates spaced by wires 0.15 mm in diameter and solidified.

MCD was measured with the laboratory made installation. The plates were placed between poles of electromagnet with the drilled cylindrical holes through which the light beam passed. Thus directions of the light beam and the magnetic field were parallel to each other and perpendicular to the plane of the plate. The light wave polarization state was modulated from the right-hand to the left-hand circular polarization relatively to the magnetic field direction. The modulator was made of a fused silica prism with a glued piezoelectric ceramic element. In the absence of an acoustic excitation, a prism was optically isotropic. When the ac voltage of frequency ω corresponding to the eigen frequency of the system was supplied to the piezoelectric ceramics, an elastic standing wave was excited in the quartz prism. Linearly polarized light with the polarization plane turned to an angle of 45° relatively the horizontal prism axis failed on the prism. At the exit of the prism, the light wave acquired circular polarization when a standing acoustic wave was excited in it. This polarization changed from the right- to the left-hand circle during one period of acoustic vibration of the prism. In the case of a sample possessing MCD, its absorption coefficients were different for the right- and left-hand circular polarized light waves with respect to the magnetic moment direction of a sample. As a result, the light flux having passed through the sample and reaching a photomultiplier had a modulated intensity. The MCD value was measured as the difference between the photomultiplier voltages for two opposite directions of an applied magnetic field in the spectral range (10-26) $\cdot 10^3$ cm^{-1} in a magnetic field of up to 1.2 T at 300 K and up to 0.5 T for lower temperatures. The

measurement accuracy was about 10^{-4}, and the spectral resolution was 20–50 cm^{-1} depending on the wavelength.

3. Results and Discussion

3.1. Nanoparticles structure, phase, and morphology

As is known, to obtain pure crystals of ferrite garnet with reproducible properties, it is necessary to provide the stoichiometric ratio of cations, Dy:Fe=3:5, and the complete precipitation of that to be achieved. Process for the obtaining precursor can be represented as follows:

$$24RX+ 3 DyA_3 + 5 FeA_3 \rightarrow 24RA + \{3 Dy X_3+ 5 FeX_3\},$$
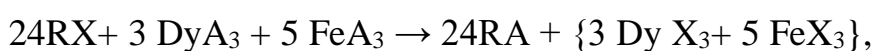
RX, RA are the anion-exchange resins (X= $1/2CO_3^{2-}$; A= $1/2SO_4^{2-}$, NO_3^-).

In our case, the precipitation of cations from the solution occurred completely, since the residual concentration of metals in the solution was less than 1 % according to the atomic absorption analysis.

Fourier transform infrared spectroscopy (FT-IR) can provide detailed information about the structure and positions of the ions in the prepared nanoparticles. The FT-IR spectrum of product synthesized at the precursor calcination temperature 850 °C is presented in Fig. 1. The major frequency band in the range between 450–600 cm^{-1} revealed the formation of single-phase garnet structure [36]. This region consists of three frequency bands: ν_1 at 652 cm^{-1} caused by the stretching vibrations of the tetrahedral iron-oxygen bond, ν_2 at 601 cm^{-1} caused by the iron -oxygen vibration in octahedral sites, and ν_3 at 564 cm^{-1} due to the dodecahedral dysprosium -oxygen bond. It should be underlined that the set of three above bands are found to be the main evidence of DyIG phase [37].

As can be seen from Fig. 2, all the detected peaks in presented XRD patterns could be indexed to the cubic phase DyIG (JCPDS (01-073-1378). The calcination temperature is known to be one of the main factors affecting in the formation of the garnet phase, and it is worth noting that in our case the calcination temperature is lower than that reported in similar works [10, 38]. It is probably concerned with the fact that the method based on anion exchange co-precipitation decreases the

temperature of the DyIG formation. Additionally, the use of hydroxides instead of oxides also decreases the temperature due to the higher reactivity of hydroxides in comparison with that of oxides.

Fig. 3 reveals the TEM images of as-prepared DyIG, indicating the sample consists of particles with size of approximately 20-30 nm. However, as shown in Fig. 3b, the particles are combined in aggregates with a size of about 100 nm. The formation of aggregates is due to the strong tendency of nanoparticles to minimize their surface energy.

3.2. *Nanoparticles magnetization field dependence*

The nanoparticles magnetization dependence on an external magnetic field recorded at T=298 K is presented in Fig. 4. Close to the rectangular shape hysteresis loop with coercivity H_c=280 Oe and, practically, linear magnetization increase with the further increase of magnetic field is observed. The hysteresis loop parameters can be compared with date presented in Ref. [39] for the DyIO nanoparticles prepared by aqueous sol-gel method using the different samples annealing temperature. At the annealing temperature 900 °C, H_c was 274 Oe and the magnetization value in magnetic field 4.4 kOe was 4.4 emu/g (Table 4 in [39]). Almost absolutely the same values describe hysteresis of nanoparticles investigated here.

Magnetic saturation is not reached up to the maximal field used 50 kOe. Such dependence is characteristic of some of the rare earth iron garnets (gadolinium, terbium, dysprosium, holmium). This phenomenon is associated with the competition of the negative exchange interaction between the rare-earth and iron sub-lattices and the applied magnetic field resulting in an appearance of the non-collinear magnetic structure over a certain interval of magnetic fields ($H_1 < H < H_2$). The field-induced non-collinear magnetic structures in REIG were predicted theoretically [40,41] and revealed experimentally at the end of 1960-s (e.g., [41,42,43], and is still the subject of the intensive research (e.g., [44]). Thus, the magnetization behavior in the high magnetic field observed for the DyIG nanoparticles synthesized is typical for the rare earth iron garnets.

3.3. *Magnetic circular dichroism*

As it was mentioned in the introduction, own of characteristic feature of the rare-earth garnets is reorganization of their magnetic structure at some compensation temperature, T_{comp}. Therefore, it is necessary to follow the temperature dependences of the properties of the investigated nanoparticles in order to evaluate their compliance with the bulk and thin-film DyIG samples. For DyIG bulk crystal $T_{comp}= (220\pm2)$ K [45], for thin film $T_{comp}=225K$ [21]. At temperatures higher than T_{comp}, the total sample magnetization should be determined by the iron sublattice, while at $T< T_{comp}$ the total magnetization will be determined by the Dy sublattice magnetic moment directed oppositely relative to the Fe sublattice magnetic moment. That is why the total magnetization becomes equal to zero at $T= T_{comp}$. As MCD is linear function of magnetization, this reordering transition should be reflected in temperature behavior of MCD too. Contrary to the commonly used magnetization measurements, advantage of the MCD technique is possibility to single out contribution from various magnetic sub-lattices.

MCD spectra of the composite sample containing DyIG nanoparticles recorded at two temperatures – significantly above and below T_{comp} of bulk or thin film samples, are presented in Fig. 5. First of all, the different sign of the MCD signal is seen at higher and lower temperature what evidences on the reorientation of the sample total magnetic moment, that is, on the magnetic compensation phenomenon in the sample. The picture is similar to that observed in Ref. [26] where MCD spectra of the $Er_3Fe_5O_{12}$ single crystal in the region of the electron transition between the ground state and the first excited state multiplets was studied in dependence on temperature. For convenience of the MCD spectra analysis, it is possible to divide them into two groups of extrema prevailing in different wave length intervals. MCD spectrum in the area of $(18-26)\cdot10^3$ cm^{-1} corresponds almost completely with the MCD spectrum presented earlier [32] for YIG nanoparticles fabricated with the same technique as well with the MCD spectrum of the YIG thin films and thin crystal plates available in literature [23, 24, 25, 46]. As YIG contain no RE elements, all MCD features in this region can be associated with

electron transitions in Fe^{3+} ions both single-ion and charge-transfer type. Note some differences in the identification of the MCD maxima with certain types of electron transitions in the works of different authors. That is why we do not indicate here the names of transitions in this region. Transitions associated with the Fe^{3+} ion occur also in the lower energy spectral region, in particular, features near 10920 and 14090 cm^{-1} due to the transitions $^6A_{1g}(^6S) \rightarrow ^4T_{1g}(^4G)$ and $^6A_{1g}(^6S) \rightarrow ^4T_{2g}(^4G)$ were observed in the $Y_3Fe_5O_{12}$ MCD spectrum in Ref. [25]. In Fig. 5, two fairly weak lines are observed at room temperature near the light wave energies 13300 and 10990 cm^{-1}, and one most intensive line centered near 12380 cm^{-1}. These energy values are characteristic for the Dy^{3+} ion transitions from the ground state multiplet $^6H_{15/2}$ to the exited state multiplets $^6F_{3/2}$, $^6F_{7/2}+^6H_{5/2}$, and $^6F_{5/2}$ [47], correspondingly. Evidently, the last one originates from the transition in the Dy^{3+} ion only, while two firsts can overlap partly with the transitions in Fe^{3+} ions. Therefore, its temperature behavior will be used to monitor the Dy sublattice temperature behavior. Since transitions in Dy^{3+} ion occur between deeper levels they are least subjected to an influence of the ion environment, and MCD maxima should be rather narrower comparing to the broad maxima observed at higher energies and due to the transitions in Fe^{3+} ion that is actually observed.

The section of the MCD spectrum near 12420 cm^{-1} is shown in Fig. 6 in dependence on temperature. As the sample is cooled, the MCD decreases, passes through zero, and after change sign its absolute value increases again. Similar temperature behavior observed for all other MCD peaks originated both from Fe^{3+} and Dy^{3+} ion transitions. In Fig. 7, temperature behavior of two MCD peaks associated with Fe and Dy sub-lattices is shown. The temperature corresponding to zero MCD value, that is, the compensation temperature T_{comp} is the same for both sub-lattices and equals to 214 K. Below T_{comp} the curves in Fig. 7 are completely identical while at temperatures higher than T_{comp} curves for Fe and Dy sub-lattices differ from each other in some extent. One can indicate that below T_{comp} the Fe and Dy magnetic sub-lattices are rigidly coupled.

Thus, the temperature changes of the MCD correspond, in principle, to the temperature changes of the magnetization in RIG observed in the works cited above. As concerns magneto-optical effects, similar temperature changes of Faraday rotation (FR) was observed in DyIG films for several wave length [21]. For the film, T_{comp} was 225 K, and the shapes of the curves FR(T) coincided with each other both above and lower 225 K. Some difference between our and Ref. [21] data can be associated with that FR of the film is strongly influenced by the overlapping dispersive shape contributions attributed to Fe^{3+} transitions while MCD maxima of dissipative form allow to separate the contributions of individual sub-lattices for the DyIG and trace their temperature dependences.

Magnetic field dependences of MCD originated from electron transitions in Fe^{3+} (at energy 20200 cm^{-1}) and Dy^{3+} (at energy 12420 cm^{-1}) ions are presented in Fig. 8 for T=300 K. For both cases, the narrow almost rectangular hysteresis loops are observed with the field of the magnetization saturation of about 2.25 and 3.8 kOe for Fe and Dy sub-lattices, correspondingly. The coercivity H_c values are of about 200 Oe. With the sample cooling up to 90 K, the H_C practically does not change. Thus, the coercivity, its temperature dependence, and the hysteresis loop shape obtained from two types of measurements technique are close with each other. However, MCD and magnetization behavior in the higher magnetic field are quite different (compare Figs. 3 and 8). This discrepancy can be associated with the fact that, like the Faraday rotation, the visible MCD is related to the individual sub-lattices magnetic moments rather than to the total magnetization. Authors of Ref. [48] studying the TbIG single crystal, have shown the FR value to be almost independent on magnetic field up to 100 kOe at room temperature. The same result was presented in Ref. [49] for FR in DyBiIG films in magnetic fields up to 20 kOe. So, the different behavior of magnetization and MCD in high magnetic fields do not contradict to data available in literature. However, this problem needs further thorough investigations which are in progress now.

The set of the results obtained allows to assert that the properties of synthesized nanoparticles are consistent with the properties of the bulk DyIG crystals.

4. Conclusions

DyIG nanoparticles were synthesized with the modified anion resin exchange precipitation method using resin in CO_3-form what provides to produce particles of smaller size as compared to usually used resin in OH-form. The nanoparticles synthesized were of the garnet structure with an excellent crystallinity. No other phases were revealed. The nanoparticles magnetization dependence on an external magnetic field as well as the magnetic field and temperature dependencies of MCD indicate that the magnetic properties of synthesized nanoparticles correspond completely to the properties of the bulk DyIG crystals with all peculiarities inherent in this material including magnetic sub-lattices compensation and strong magnetization increase in high magnetic fields. The contribution of rare-earth Dy ions to the MCD was studied here for the first time. This result can be used for more rigorous studying properties of rare-earth garnets in the region of magnetic compensation temperature.

Figure captions

Fig1. FT-IR spectrum of DyIG nanoparticles.

Fig.2. X-ray diffraction pattern of DyIG nanoparticles.

Fig. 3. TEM images of nanoparticles with different magnification.

Fig. 4. Magnetization field dependence of DyIG nanoparticles at temperature 298 K. Inset: The hysteresis loop in lower fields.

Fig. 5. MCD spectra of composite sample containing $DyIG_2$ nanoparticles at temperatures 90 (full circles) and 297 (empty circles) K. H=3.5 kOe.

Fig. 6. MCD maximum associated with the transition $^6H_{15/2} \rightarrow ^6F_{5/2}$ of Dy^{3+} ion at different temperatures. H=3kOe. $T_{comp} \approx 215$ K.

Fig. 7. Temperature dependencies of the MCD intensity in the Fe^{3+} transitions region (area under the curve in the energy interval 20660-22200 cm^{-1}) and in the Dy^{3+} transition (the distance between two extrema, as it is shown in Inset in Fig. 6). H=3kOe.

Fig. 8. MCD hysteresis loops for (a) 20200 cm^{-1} (Fe sub-lattice) and (b) 12420 cm^{-1} (Dy sub-lattice) at the 297K.

References

[1] H.S. Yonder and M.L Keith, Am. Mineral 36 (1951) 519.

[2] F. Bertaut and F. Forret, Compt. Rend. 242 (1956) 382.

[3] S. Geller and M.A. Gilleo, Acta Cryst. 10 (1957) 239.

[4] F. Bertaut and R. Pauthenet, Proc. IEEE 104 B (1957) 261.

[5] K. Sadhana, S.R. Murthy, K. Praveena, Materials Science in Semiconductor Processing 34 (2015) 305.

[6] T. Ramesh, R.S. Shinde, S.R. Murthy, J. Magn. Mag. Mater. 324 (2012) 3668.

[7] G.M. Yang, J. Wu, J. Lou, M. Liu, N.X. Sun, IEEE Trans. Magn. 49 (2013) 5063.

[8] A.R. Prokopov, P.M. Vetoshko, A.G. Shumilov, A.N. Shaposhnikov, A.N. Kuzmichev, N.N. Koshlyakova, V.N. Berzhansky, A.K. Zvezdin, V.I. Belotelov, J. All. Comp. 671 (2016) 403.

[9] V.K. Sankaranarayanant and N.S. Gajbhiye, J. Phys: Condens. Matter 4 (1992) 4857.

[10] M.A. Ahmed, S.T. Bishay, S.I. Eldek, Materials Chemistry and Physics 126 (2011) 780.

[11] Z. Cheng, H. Yang, Y. Cui, L. Yu, X. Zhao, S. Feng, J. Magn. Magn. Mater. 308 (2007) 5.

[12] H. Xu, H. Yang, W. Xu, L. Yu, Current Appl. Phys. 8 (2008) 1.

[13] R. Pena-Garcia, A. Delgado, Y. Guerra, B. V. M. Farias, D. Martinez, E. Skovroinski, A. Galembeck, E. Padrón-Hernández, Phys. Stat. Sol. A-Appl. Mater.Sci.   213 (2016) 2485.

[14] K. Praveen, K. Sadhan, S. Srinath, S.R. Murthy, Mater. Res. Innov. 18 (2014) 1.

[15] M. Guillot, C.N. Chinnasamy, J.M. Greneche, and V.G. Harris, J. Appl. Phys. 111 (2012) 07A517.

[16] P.J. Stephens, J. Chem. Phys. 52 (1970) 3489.

[17] R. Kripal, M. J. Bajpai, All. Comp. 490 (2010) 5.

[18] G.A. Gehring, M.S.Alshammari, D.S. Score, J.R. Neal, A. Mokhtari, A.M. Fox, J. Magn. Magn. Mater. 324 (2012) 3422.

[19] M. Ying, W. Dizayee, Z.X. Mei, X.L. Du, A.M. Fox, and G.A. Gehring, J. Phys D –Appl. Phys 48 (2015) 255502.

[20] H. Umezawa, Y. Yokoyama and N. Koshizuka, J. Appl. Phys. 63 (1988) 3113.

[21] J. Ostoréro, M. Escorne, A. Pecheron-Guegan, F. Soulette, and H. Le Gall, J. Appl. Phys.75 (1994) 6103.

[22] M. Guillot, H. Le Gall, J. Gouzerh, J.M. Desvignes, and M. Artinian, J. Appl. Phys. 79 (1996) 5932.

[23] J.C. Canit, J. Badoz, B. Briat, and R. Krishnan, Solid State Commun. 15 (1974) 767.

[24] S. Visnovsky, J.C. Canit, B. BriaT, R. Krishnan, J. Physique 40 (1979) 73.

[25] G.B. Scott, D.E. Lacklison, H.I. Ralph, and J.L. Page, Phys. Rev. B 12 (1975) 2562.

[26] P.G. Feldmann, H. Le Gall, and M. Guillot, IEEE Trans. Magnetics MAG-21 (1985) 1669.

[27] K.K. Kefeni, T.A.M. Msagati, B.B. Mamba, Mater. Sci. Eng. B 215 (2017) 37.

[28] S.V. Saikova, M.V. Panteleeva, G.L. Pashkov, R.B. Nikolaeva, Zhurnal prikladnoi khimii (2002) 1823 (in Russian).

[29] G.L. Pashkov, S.V. Saikova, M.V. Panteleeva, E.V. Linok, Theoretical Foundations of Chemical Engineering 48 (2014) 671.

[30] G.L. Pashkov, S.V. Saikova, M.V. Panteleeva, E.V. Linok, A. S. Samoilo, G. N. Bondarenko, Glass and Ceramics 70 (2013) 225.

[31] G.L. Pashkov, S.V. Saikova, M.V. Panteleeva, E.V. Linok, I.V. Korol'kova, Glass and Ceramics 71 (2014) 57.

[32] G.L. Pashkov, S.V. Saikova, M.V. Panteleeva, E.V. Linok, P.D. Ivantsov, A.M. Zhizhaev, Izv. Vyssh. Uchebn. Zaved. Khim. Khim. Tekhnol. 5 6 (2013) 77 (in Russian).

[33] G.L. Pashkov, S.V. Saikova, M.V. Panteleeva, E.V. Linok, N.P. Evsevskaya, G.N. Bondarenko, A.M. Zhizhaev, L.S. Tarasova, Glass and Ceramics 73 (2016) 107.

[34] G.L. Pashkov, N.P. Evsevskaya, E.V. Linok, M.V. Panteleeva, G.N. Bondarenko, Journal of Siberian Federal University. Chemistry 9 (2016) 371.

[35] G.L. Pashkov, S.V. Saikova, M.V. Panteleeva, Theoretical Foundations of Chemical Engineering 50 (2016) 575.

[36] A. Katelnikovas, A. Kareiva, Low-temperature synthesis of lutetium galliumgarnet (LGG) using sol–gel technique, Mater. Lett. 62 (2008) 1655.

[37] R. Tholkappiyan, K. Vishista, Applied Surface Science 351 (2015) 1016.

[38] G. Rekha, R. Tholkappiyan, K. Vishista, F. Hamed, Applied Surface Science 385 (2016) 171.

[39] O. Opuchovic, A. Kareiva, K. Mazeika, D. Baltrunas, J. Magn. Magn. Mater, 422 (2017) 425.

[40] S.V. Tyablikov, Metody kvantovo1 teorii magnetizma (Methods of the Quantum Theory of Magnetism), Nauka, 1965.

[41] A. Clark and E. Callen, J. Appl. Phys. 39 (1968) 5972.

[42] K.P. Belov, E.V. Talalaeva, L.A. Chernikova, R.Z. Levitin, T.V. Kudryavtseva, S. Amadezi, V.I. Ivanovski1, Zh. Eksp. Teor. Fiz. 58 (1970) 1923; Soviet Phys.-JETP 31 (1970) 1035.

[43] J. Schelling and A. Clark, Phys. Lett. 29A (1969) 172.

[44] M. Lahoubi, W. Wang, J. Magn. Magn. Mater. 393 (2015) 437.

[45] F. Bertaut and R. Pauthenet, Proc. IEE 104 b (1957) 261.

[46] J.C. Canit, R. Krishnan, and B. Briat, Sol. St. Commun. 42 (1982) 653.

[47] P. Gorlich, H. Karras, G. Kotitz, R. Lehmann, Phys. Stat. Sol. 5 (1964) 437.

[48] F.M. Yang, N. Miura, G. Kido, S. Chikazumi, J. Phys. Soc. Japan 48 (1980) 71.

[49] M. Guillot, H. Le Gall, J. M. Desvignes, M. Artinian, J. Appl. Phys. 81 (1997) 15.